Research and development for low noise front-end electronics

Szymon Kulis
AGH University of Science and Technology
Al. Mickiewicza 30, 30-059 Krakow, Poland
Email: szymon.kulis@gmail.com

The aim of this research was to develop spectroscopic readout electronics for sensors measurements. It has been shown that using only standard components from the shelf it is possible to build spectrometric electronics with an equivalent noise charge of $212e^-$*. In this paper the author presents all theoretical contemplation, hardware realization and measurements results.*

1 Introduction

The task is to develop a preamplifier for solid state sensors. Such sensors vary with their capacitance in the range of a few pF to several hundred pF. The preamp should be able to detect signals of up to several MIPs (eg. for silicon $1MIP \simeq 4fC \simeq 25000e^-$). To achieve a good energy resolution the ENC (Equivalent Noise Charge) should be in the range of a few hundred electrons. To avoid pileups and baseline shifts the electronics should be as fast as possible. The whole system should have four channels to provide for simultaneous readout of up to four independent sensors. A Charge-to-Digital Converter (CAEN V965) should be used as digitization device. The circuit should be assembled on a printed circuit board with discrete elements. Requirements on power dissipation were not taken.

2 Architecture

From the specifications above the general concept of the readout electronics was outlined as shown in fig. 1. The main blocks of the signal chain are: preamplifier, shaper, gain and level converter block, gated integrator and analog to digital converter (QCD - Charge-to-Digital Converter) and computer software.

The preamplifier detects signals from a sensor, the shaper amplifies and shapes them in order to obtain the required signal to noise ratio. Finally, the QCD stores the pulse amplitudes.

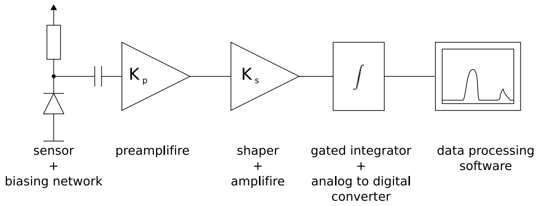

Fig. 1: *System overview.*

The memorized amplitudes are processed in a dedicated software on the PC side.

2.1 Preamplifier

Let's start our contemplation from a general diagram of a current to voltage converter wich is shown on fig. 2a. Assume that the open loop gain K_u of the amplifier doesn't depend on the frequency. For such a circuit one can write a system of equations :

$$\begin{cases} I_i(s) = I_f(s) + I_b(s) \\ V_x(s) - V_f(s) - V_o(p) = 0 \\ V_f(s) = I_f(s)Z_f(s) \\ V_x(s) = V_b(s) = I_b(s)Z_b(s) \\ V_o(s) = -K_v V_x(s) \end{cases} \tag{1}$$

The solution is :

$$V_o(s) = -\frac{I_i(s)}{\frac{1}{Z_f(s)} + \frac{\frac{1}{Z_f(s)}+\frac{1}{Z_b(s)}}{K_v}} \tag{2}$$

To achieve a linear response of the circuit impedances should be capacitive (fig. 2b). In this case (2) can be rewritten as:

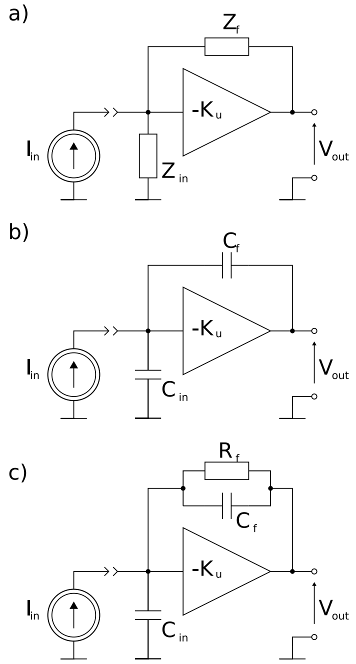

Fig. 2: *Preamplifier a) general current to voltage converter b) capacitive feedback c) resistive and capacitive feedback*

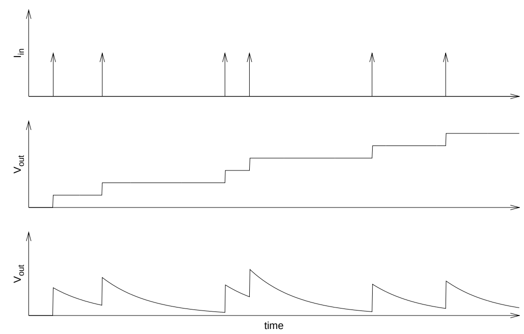

Fig. 3: *Preamplifier response a) input pulses b) capacitive feedback c) resistive and capacitive feedback*

$$V_o(s) = -\frac{I_i(s)}{s}\frac{K_v}{(K_v+1)C_f + C_b} \tag{3}$$

Our input signal derives from the sensor, so we can assume that:

$$I_i(t) = Q_i\delta(t) \tag{4}$$

where Q_i is the charge of the input pulse. Equation (4) can be transformed to the Laplace domain as:

$$I_i(s) = Q_i \tag{5}$$

On such an input pulse the preamplifier's response is:

$$V_o(s) = -\frac{Q_i}{s[C_f + \frac{C_f+C_b}{K_v}]} \tag{6}$$

and thus in the time domain:

$$V_o(t) = -\frac{Q_i}{C_f + \frac{C_f+C_b}{K_v}} \longrightarrow V_o(t) = -\frac{Q_i}{C_f} \tag{7}$$

A Dirac pulse at the input gives a Heaviside step at its output. If the open loop gain is high enough the amplitude of this step doesn't depend on the input capacitance. It is proportional to the injected charge and reversely proportional to the feedback capacitance.

During normal operation the sensor generates a stochastic train of pulses. The response of the preamplifier on such an input signal is presented in fig. 3b. After a few pulses the preamplifier's output is saturated. To avoid this saturation effect one can add a resistor (see fig. 3c) in the feedback loop. Repeating the calculations and calling $\tau_f = R_f C_f$ and $\tilde{C} = \frac{C_f(K_v+1)+C_d}{K_v}$ we get:

$$V_{orf}(s) = -\frac{Q_i}{s\tilde{C}\left[\frac{1}{\tilde{C}R_f} + s\right]} \tag{8}$$

and in the time domain:

$$V_{orf}(t) = -\frac{Q_i}{\tilde{C}}e^{-\frac{t}{\tilde{C}R_f}}$$

$$\longrightarrow V_{orf}(t) = -\frac{Q_i}{C_f}e^{-\frac{t}{\tau_f}} \tag{9}$$

2.2 Shaper

One of the simplest shaping circuits consists of only one differentiation. It is shown in fig. 4a. As will be shown later, it has a very good noise performance as well. The transfer function of such a circuit is:

$$\frac{V_o(s)}{V_i(s)} = \frac{s}{s + \frac{1}{R_d C_d}} \tag{10}$$

With $\tau_d = R_d C_d$ the response of the shaper to a Heaviside step with an amplitude A_i in the time domain is:

$$V_o(t) = A_i e^{-\frac{t}{\tau_d}} \tag{11}$$

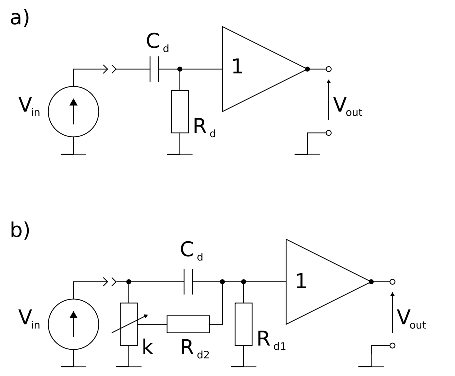

Fig. 4: *Shaper a) ideal b) with PZC.*

Unfortunately, we don't have an ideal voltage step at the output of our preamplifier. In fact it is an exponential function (9). The response to such an input signal of our shaping network is bipolar (with long negative tail). To avoid this tail one can build a so called pole-zero-cancellation circuit (PZC).The schematic diagram of a PZC circuit is shown in fig. 4b. The transfer function of such a circuit can be written as:

$$F\left(s\right)=\frac{s+\frac{k}{R_1C}}{s+\frac{R_1+R_2}{R_1R_2C}} \tag{12}$$

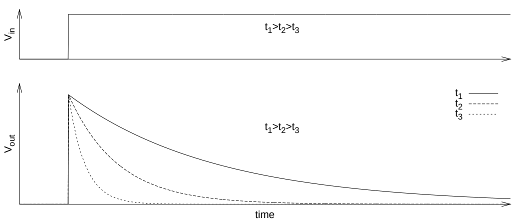

Fig. 5: *Shaper response a) input step b) output.*

Merging (8) and (12) gives the output voltage of the shaping network:

$$\begin{aligned} V_{out}(s) = V_{orf}\left(s\right)F\left(s\right) = \\ -\frac{Q_i}{s\tilde{C}\left[\frac{1}{\tilde{C}R_f}+s\right]}\frac{s+\frac{k}{R_1C}}{s+\frac{R_1+R_2}{R_1R_2C}} \end{aligned} \tag{13}$$

With $\frac{1}{\tilde{C}R_f}=\frac{k}{R_1C}$ and $\tau_d=\frac{R_1+R_2}{R_1R_2C}$ we have a response exactly equal to (11). In the further contemplation we assume that the preamplifier and the shaper response are given by (11).

2.3 Gain stage

To match the amplitude of the output pulse with the QCD input it is necessary to amplify the pulse. For different sensors (and biasing techniques) input pulses can have negative or positive polarity. Because the given QCD can handle only negative pulses it is necessary to add the possibility to invert the pulse. For this purpose one can use either an inverting (fig. 6 a) or a noninverting (fig. 6b) configuration of an operational amplifier.The transfer function for the inverting configuration is:

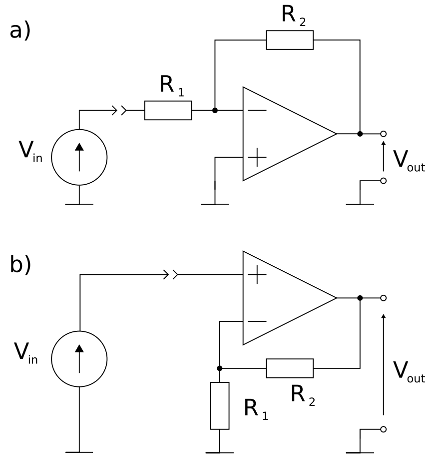

Fig. 6: *Gain stage a) invertering b) non invertering*

$$\frac{V_o(s)}{V_i(s)}=-\frac{R_2}{R_1} \tag{14}$$

and correspondingly for the noninverting configuration:

$$\frac{V_o(s)}{V_i(s)}=\left(1+\frac{R_2}{R_1}\right) \tag{15}$$

One can see that the gain depends only on the ratio R_2/R_1.

2.4 Gated integrator

Fig. 7 shows the principle schematic diagram of a gated integrator:

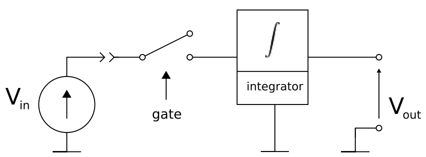

Fig. 7: *Gated integrator*

During the active interval t_g (when the gate switch is closed) input and output of the integrator follow the function:

$$V_o(t) = \int V_i(t)dt \tag{16}$$

Normally t_g would be adjusted in a way to obtain the best compromise between noise and shaping time. If the gate switch closes at the begin of the pulse, the pulse is entirely integrated. We can write:

$$V_o(t) = \frac{Q}{C}\int_0^{T_m} e^{-\frac{t}{\tau_d}}dt = \frac{Q\tau_d}{C}(1 - e^{-\frac{T_m}{\tau_d}})dt \tag{17}$$

One can see that if the gate is left closed the output voltage will reach the limiting value $\frac{Q\tau_d}{C}$.

2.5 Charge adapter

The system functionality is checked with test pulses at the input. To generate such a test pulse one can use a charge injector which is shown in fig. 8.

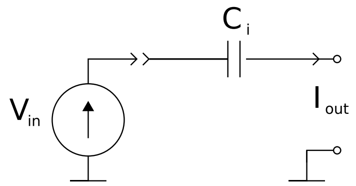

Fig. 8: *Charge adapter*

Assuming that this adapter is connected to a low impedance input a voltage step at the input results in a Dirac like current pulse transfering a charge:

$$I_o(s) = \pm A_i \cdot C_i \tag{18}$$

where A_i is the amplitude of the input step. The width of the output pulse depends mostly on the rise time of the input pulse (therefore the rise time of the input pulse should be as short as possible).

2.6 Full channel

The ideal schematic diagram of a full channel is shown in fig. 9.

3 Noise performance

3.1 Model

Analyzing noise of a whole system is to complicated, therefore a few assumptions must be taken. All components except amplifier, feedback loop and sensor are considered to be noiseless (this assumption is quite good if the gain of the preamplifier is high enough). This way the amplifier's noise is represented by a serial noise voltage generator and a shunt noise current generator. They are assumed to be uncorrelated and to have a white noise spectrum each. Flicker ($1/f$) noise is neglected. In parallel to the shunt noise current generator from the preamplifier one has also contributions from the dark current of the sensor (leakage current) and the feedback resistor. The simplified model is shown in fig. 10. In this equation C represents the sum of capacitances of the sensor, the input capacitance of the preamplifier and the feedback capacitance.

Under this assumption the equivalent serial(voltage) noise is given by:

$$\frac{v_n}{df} = \frac{v_{pre}}{df} = a \tag{19}$$

and the parallel (current) noise by:

$$\frac{i_n}{df} = \frac{i_{pre}}{df} + 2qI_d + \frac{4kT}{R_f} = b \tag{20}$$

where:
$\frac{v_{pre}}{df}$ - serial noise of preamplifier
$\frac{i_{pre}}{df}$ - parallel noise of preamplifier
I_d - leakage current of sensor
R_f - feedback resistor
k - Boltzmann's constant
T - temperature (K)
df - frequency interval

3.2 Analysis

The knowledge of the spectral density of the noise is useful when we want to calculate the mean squared fluctuation in the associated networks.

Lets have a look on the effect of such virtual noise input pulses arising during a specific period of time. Each source is a generator of stochastic voltage or current pulses. As it is shown in [4], a random pulse sequence with the mean rate n and amplitude η is equivalent to white noise with a spectral density of mean square value of $2n\eta^2$ (per second).

Campbell's theorem says that the total output fluctuation is the result of the superposition of the separate independent random fluctuations

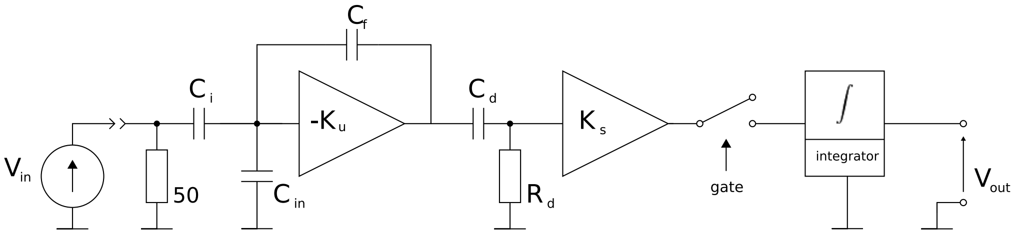

Fig. 9: *Idealized schematic diagram of a full channel*

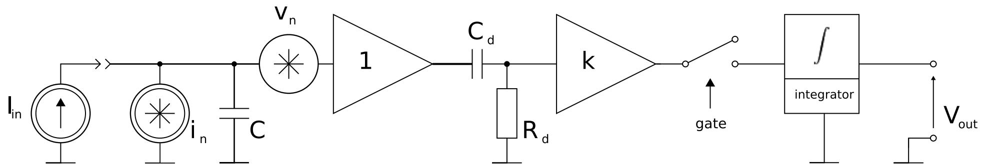

Fig. 10: *Noise modeling circuit*

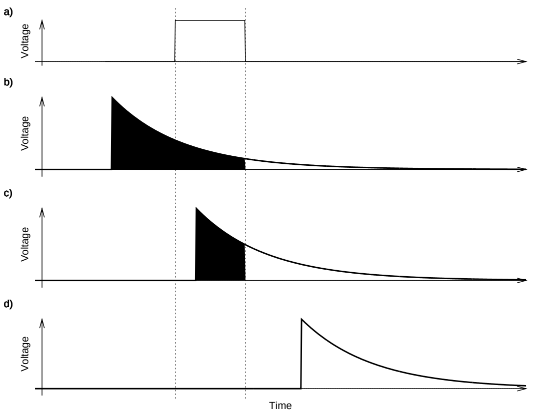

Fig. 11: *a) gate b) "early" noise pulse c) noise pulse arising t_d d) "late" noise pulse*

occurring within the measurement time due to the variations described above:

$$< v_{ng}^{\bar{2}} > = \int [v_{ng}(t)]^2 n dt \tag{21}$$

Let's have a look onto the arrival of a single electron at the input at time t_0.

$$v_p(t, t_o) = \begin{cases} 0 & t < t_0 \\ \frac{q}{c} e^{-\frac{t-t_0}{\tau_d}} & t > t_0 \end{cases} \tag{22}$$

Puting this shape into (16) and assuming that the gate switch is closed at the time $t = 0$ (see fig. 11) we get:

$$v_{ng}(t_o) = \begin{cases} a \int_{t=0}^{t_g} \frac{q}{c} e^{-\frac{t-t_0}{\tau_d}} dt & t_0 < 0 \\ a \int_{t=t0}^{t_g} \frac{q}{c} e^{-\frac{t-t_0}{\tau_d}} dt & 0 < t_0 < t_g \\ 0 & t_0 > t_g \end{cases} \tag{23}$$

The total grid current output noise $< v_{ng}^{\bar{2}} >$ can be calculated using formula (21) and integrating with respect to t_0 over the whole period from $-\infty$ to t_g.

$$< v_{ng}^{\bar{2}} > = \begin{cases} \left(\frac{kq\tau_d}{C}\right)^2 \int_{t_0=-\infty}^{0} e^{-\frac{2t_0}{\tau_d}} (1 - e^{-\lambda})^2 dt_0, t_0 < 0 \\ \left(\frac{kq\tau_d}{C}\right)^2 \int_{t_0=0}^{t_g} e^{-\frac{2t_0}{\tau_d}} (1 - e^{-\lambda})^2 dt_0, 0 < t_0 < t_g \\ 0, t_0 > t_g \end{cases} \tag{24}$$

where $\lambda = t_g/\tau_d$. Adding all cases we get a total grid noise present at the integrator's output as:

$$< v_{ng}^{\bar{2}} > = \frac{k^2 q b \tau_d^3}{2C^2} \left(\lambda - 1 + e^{-\lambda}\right) \tag{25}$$

Repeting the calculations for the shunt noise we get:

$$< v_{ns}^{\bar{2}} > = \frac{k^2 a \tau_d}{2} \left(1 - e^{-\lambda}\right) \tag{26}$$

The total output mean square voltage noise is given by the sum of grid (25) and shunt noise (26) and is equal to:

$$< v_n^{\bar{2}} > = \frac{k^2 \tau_d^2}{2} \left(\frac{b t_d}{C^2} \left(\lambda - 1 + e^{-\lambda}\right) + \frac{a}{t_d} \left(1 - e^{-\lambda}\right) \right) \tag{27}$$

On the other hand one electron appearing at the input at time $t = 0$ gives at the output:

$$v_s^{\bar{2}} = \left(\frac{k \tau_d q}{C}\right)^2 \left(1 - e^{-\lambda}\right)^2 \tag{28}$$

From the ratio of equations (27) and (28) the equivalent noise charge present at the input is equal to:

$$ENC = \frac{C}{q\sqrt{2}} \frac{\sqrt{\frac{a\tau_d}{C}\left(\lambda - 1 + e^{-\lambda}\right) + \frac{b}{\tau_d}\left(1 - e^{-\lambda}\right)}}{\left(1 - e^{-\lambda}\right)} \tag{29}$$

In our design we can easily modify τ_d and t_g. To find the minimum of this function (31) we can assume (for a while) that ratio of τ_d and t_g is constant. In this case the whole expression has a minimum if:

$$t_d = C\sqrt{\frac{b}{a}\frac{1 - e^{\lambda}}{\lambda - 1 + e^{-\lambda}}} \tag{30}$$

thus the ENC formula can be rewritten as:

$$ENC =$$

$$\frac{2\sqrt{C}}{q}\left(\frac{ab}{4}\right)^{1/4}\left(\lambda - 1 + e^{-\lambda}\right)^{1/4}\left(1 - e^{-\lambda}\right)^{-3/4} \tag{31}$$

This expression has its minimum for $\lambda \simeq 1.04$, this means that shaping time and integration time should be almost identical.

4 Realization of the final circuit

4.1 Schematic diagram

Basing on the theoretical contemplation the circuit prototype was developed. The full schematic diagram is shown in appendix 1. The operational amplifier OP657 (Texas Instruments) was chosen due to its very good noise performance and its high gain bandwidth product.

To make the serial noise as small as possible the resistance of the feedback resistor R_f was chosen as high as possible ($5G\Omega$). In order to increase the gain the feedback capacitance c_f should be as small as possible. It was decided not to mount this capacitor at all and to use the stray capacitance only.

Let's apply our noise model to this circuit configuration. From the datasheet of the OPA657 we find its voltage noise to be:

$$a = \frac{v_{pre}}{df} = 4.7\frac{nV}{\sqrt{Hz}} \tag{32}$$

and the current noise:

$$\frac{i_{pre}}{df} = 1.3\frac{fA}{\sqrt{Hz}} \tag{33}$$

additionaly we have current noise from R_f ($5G\Omega$):

$$\frac{4kT}{R_f} = 1.0\frac{fA}{\sqrt{Hz}} \tag{34}$$

while the sensor current is neglected. Summing (34) and (33) we have :

$$b = 2.3\frac{fA}{\sqrt{Hz}} \tag{35}$$

The input capacitance of the preamplifier is assumed to be $5.2pF$ (datasheet), test capacitance is $1pF$ and wiring capacitance in front of it wasn't measured but is calculated to be $2pF$. Thus the effective "noise capacitance" C is equal to $8.2pF$. We can plot the ENC as a function of t_g and t_d (31). Using the values investigated above the results are presented in fig. 12 .

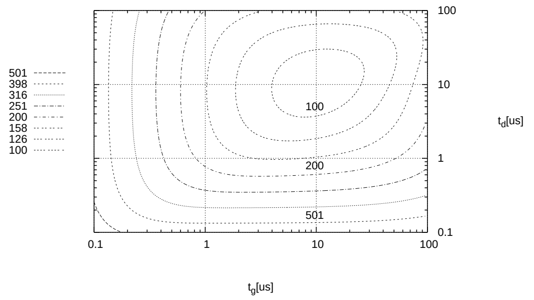

Fig. 12: *ENC as a function of t_g and t_d. (using theoretical model parameters)*

Analyzing this plot one can find that the optimum ENC is found for $t_g = t_d = 10\mu s$.

The shaper is designed using an AD8012 opamp (low noise, high speed). By means of the jumper J3 it is possible to switch polarity of the output pulse, both, J1 and J2, are used to switch the polarity. Possible gain and polarity combinations are shown in fig 13. By means of the potentiometer P3 the output DC offset can be adjusted.

The aim of U1 and U2 is to deliver stable supply voltages. The resistors R_1 - R_4 and R_{test} are mounted to match the impedance of the connection cables.

4.2 Printed circuit board

The developed printed circuit board carries four channels of the developed preamplifier chain. Its

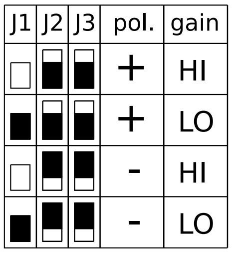

Fig. 13: *Gain / polarity jumpers modes*

dimensions are $130x125mm^2$. It fits in the box of a given setup [6]. Output and input connectors are placed in the way that they are compatible with previously used preamplifiers. It is foreseen to mount additional shieldings. The PCB project is attached in appendix 2.

5 Measurement setup

To improve the measurement procedure a special measurement environment was prepared. The block diagram is shown in fig 14. All devices are remotely controlled from a Personal Computer with dedicated software. The software is written in C++ and described in [7]. Almost all measurements are performed automatically, the data are processed immediately after the measurement and a report file in HTML format containing raw data and results is written.

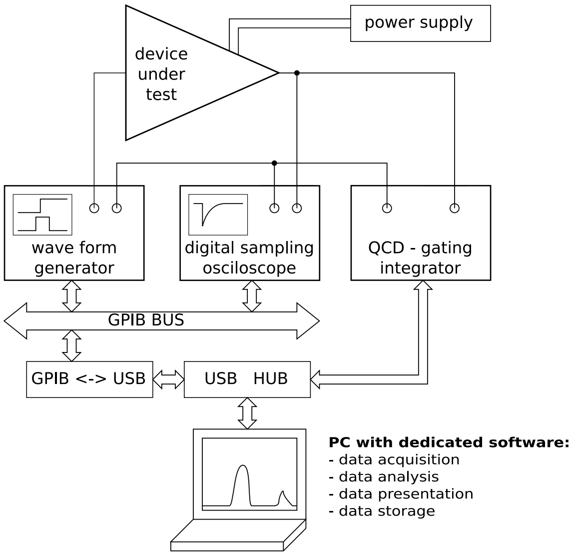

Fig. 14: *Measurement setup.*

6 Measurements results

6.1 Preamplifier

Fig. 15 shows a typical response of the preamplifier for different input charges.

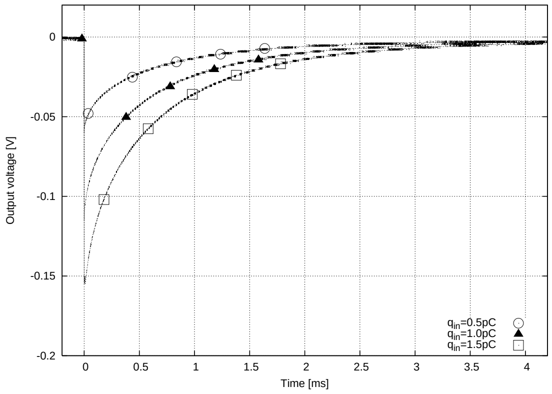

Fig. 15: *Response of preamp to different input charges.*

The output voltage as a function of the input charge is shown in fig. 16. The circuit is linear and deviations are smaller than 0.3%. The gain measured is $11.6V/pC$. The feedback capacitance is estimated to be $C_f = 86fF$. With a feedback resistor of $R_f = 5G\Omega$ we get a time constant τ_f of $0.43ms$ witch is also documented in fig. 15.

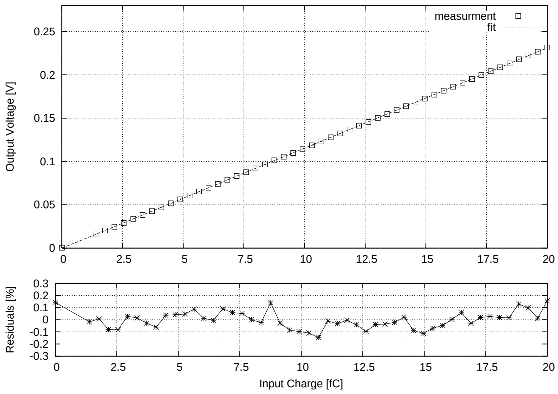

Fig. 16: *Linearity of the preamplifier.*

The rise time of the preamplifier as a function of the input capacitance is shown in fig. 17. For the measured range of input capacitances the output rise time is less then $50ns$. With higher capacitances this circuit starts to oscillate, so a precise measurement of the corresponding rise time was impossible. From the figures discussed we can conclude that the shaping time should

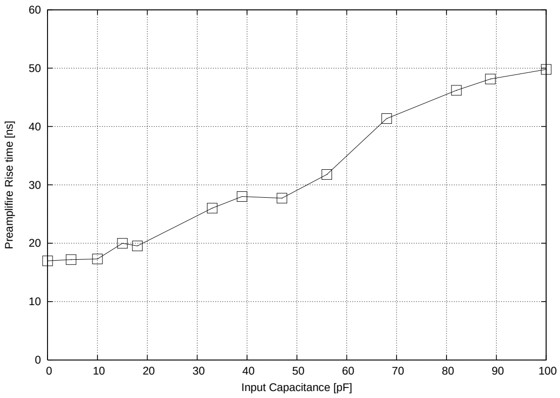

Fig. 17: *Output rise time of preamplifier vs input capacitance.*

be longer than $500ns$ (one order of magnitude larger than the preamp's rise time). Thus the shaping network behaves the same way as for a step function at the input.

6.2 Noise

After first measurements ($10\mu s$ shaping time) the observed shunt noise was much higher than expected ($400e^-$ measured instead of $150e^-$ expected).

The influence of the shunt noise could be decreased by lowering the shaping time (see eq. (29)). The optimum was found witch $1\mu s$ shaping time . The ENC as a function of t_g for different t_d is shown in fig. 18. The straight lines

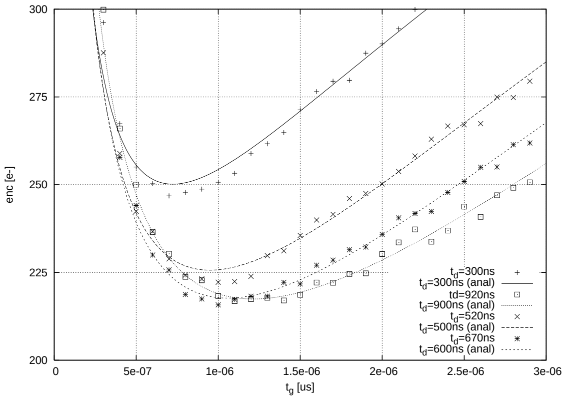

Fig. 18: *ENC as a function of t_g for a different t_d.*

are the theoretical fit. Using this fit one can determine model parameters such as:

$$
\begin{aligned}
a &= 3.4\frac{nV}{\sqrt{Hz}} \\
b &= 32.3\frac{fA}{\sqrt{Hz}} \\
C &= 8.2pF
\end{aligned}
\tag{36}
$$

The voltage noise and the input capacitance fit nicely to those expectations.

The current noise is one order of magnitude higher than expected. One reason is the bias current of the inputs of the operational amplifier. The maximum input bias current of the opamp used is specified to be $5nA$. Due to formula (20) this gives approximately $40\frac{fA}{\sqrt{Hz}}$ what is even higher than our model fit. Additionally systematic noise was observed in the lab. It was impossible to separate this noise.

For the parameters found the ENC formula (31) can be replotted. The results are shown in fig. 19 .

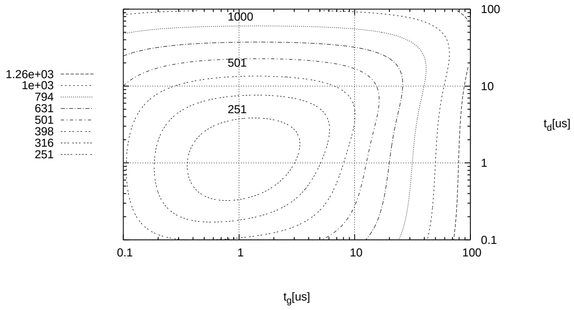

Fig. 19: *ENC as a function of t_g and t_d. (using fitted model parameters)*

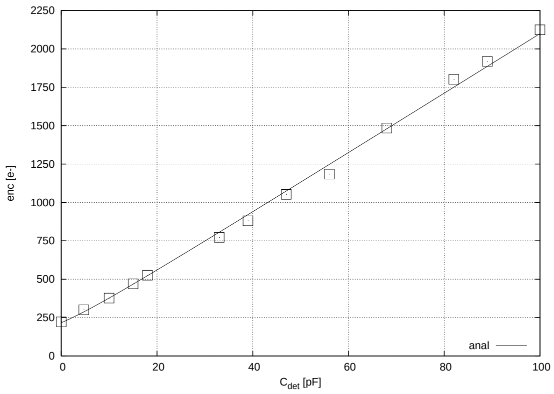

Fig. 20: *ENC vs c_{det} ($t_d = t_g = 1us$).*

As a compromise between speed and noise performance $t_g = 1us$ and $t_d = 500ns$ were chosen. For such settings the ENC measurement as a function of C_{det} was performed, results are presented in fig. 20.

As one can see from formula (31) for large enough values of C the voltage noise is dominating. The noise depends almost linearly on C. The theoretical prediction fits very well with the measurement results. The measured ENC value is $212e^-$ for zero input capacitance. The measured noise slope is $19.2e^-/pF$.

The dependence of gain from input capacitance was measured. The normalized gain as a function of C_{det} is shown in fig. 21. Analyzing

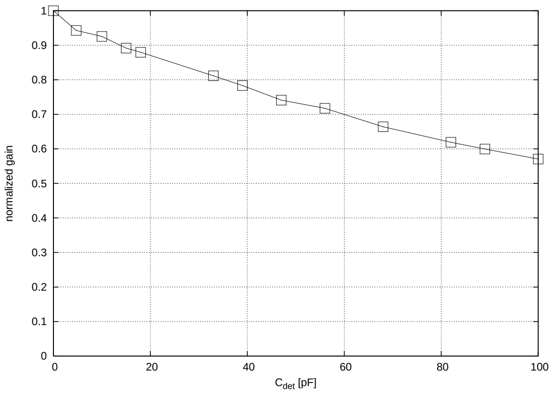

Fig. 21: *Gain vs c_{det} ($t_d = t_g = 1\mu s$).*

formula (7) one can conclude that we didn't realize a large enough value of the virtual input capacitance. The reason is the very small feedback capacitance and a limited gain bandwidth product of the given amplifier.

This behavior has no influence on the application of the amplifier because C_{det} is constant (a calibration measurement will be taken for each individual sensor anyway).

7 Summary

It has been shown that using only standard components from the shelf it is possible to build a spectrometric amplifier with an equivalent noise charge of $212e^-$. This paper presents all theoretical contemplations, the hardware realization and the measurement results of the final circuit are presented. A short overview of the circuit parameters is given in Tab. 1 . A user's manual is included in appendix 3.

Tab. 1: *Circuit performance*

parameter		value	unit
ENC		212	$[e^-]$
Noise slope		19.2	$[e^-/pF]$
shaping time		500	$[ns]$
gain	preamp	11.6	$[V/pC]$
	shaper pos. low	0.02	$[LSB/e]$
	shaper pos. high	0.1	$[LSB/e]$
	shaper neg. low	-0.02	$[LSB/e]$
	shaper neg. high	-0.1	$[LSB/e]$
power	$+5V$	110	$[mW]$
	$-5V$	110	$[mW]$

Acknowledgments

I would like to thank DESY for offering me the summer student program. Special thanks go to Wolfgang Lange for being my supervisor and helping me every time I needed it. Thanks to the whole LC group, especially to Petty Bernitt, Hans Henschel, Martin Ohlerich and Christian Grah for a very nice cooperation. I'm also very grateful to Mr Karlheinz Hiller and Mrs Sabine Bear for perfect organization.

References

[1] K. Korbel, *Uklady Elektroniki front-end*, (Uczelniane Wydawnictwo Naukowo-Dydaktyczne AGH, Krakw, 2000).

[2] K. Korbel, *Filtracja sygnalu w spektrometrycznym torze pomiarowym*, (Uczelniane Wydawnictwa AGH, Krakw, 1992).

[3] E. Gatti, P.F. Manfredi, *Processing the signals from Solid-State Detectors Elementary-Particle Physics*, (1985).

[4] M.O. Deighton, *Calculation of noise/signal ratio of a nuclear pulse amplifier employing gated active integration*, (1967).

[5] Paul R. Gray, *Analysis and Design of Analog Integrated Circuits* (Wiley, 2001).

[6] E. Kuznetsova, *"Design Studies and Sensor Tests for the Bea, Calorimeter of the ILC Detector"*, PhD thesis, Humboldt University of Berlin, 2006 DESY-THESIS-2007-10

[7] Sz. Kulis, *"Calibration software - user manual"*